

Quantum Monte Carlo simulation of spin-polarized tritium

I. Bešlić¹, L. Vranješ Markić^{1,2}, J. Boronat³

¹ Faculty of Science, University of Split, HR-21000 Split, Croatia

² Institut für Theoretische Physik, Johannes Kepler Universität, A 4040 Linz, Austria and

³ Departament de Física i Enginyeria Nuclear, Campus Nord B4-B5, Universitat Politècnica de Catalunya, E-08034 Barcelona, Spain

(Dated: November 21, 2018)

The ground-state properties of spin-polarized tritium $T\downarrow$ at zero temperature are obtained by means of diffusion Monte Carlo calculations. Using an accurate *ab initio* $T\downarrow$ - $T\downarrow$ interatomic potential we have studied its liquid phase, from the spinodal point until densities above its freezing point. The equilibrium density of the liquid is significantly higher and the equilibrium energy of $-3.664(6)$ K significantly lower than in previous approximate descriptions. The solid phase has also been studied for three lattices up to high pressures, and we find that hcp lattice is slightly preferred. The liquid-solid phase transition has been determined using the double-tangent Maxwell construction; at zero temperature, bulk tritium freezes at a pressure of $P = 9(1)$ bar.

PACS numbers: 67.63.Gh, 67.80.fh

I. INTRODUCTION

Spin-polarized hydrogen ($H\downarrow$), and its isotopes spin-polarized deuterium ($D\downarrow$) and tritium ($T\downarrow$), are fully quantum systems with a wealth of interesting properties. The low mass of $H\downarrow$ and the very weak attractive part of its interaction potential makes possible that it remains in a stable gas phase even in the limit of zero temperature. Recent microscopic calculations at zero temperature have shown that the gas phase persists for pressures up to 170 bar.¹ The gaseous state of bulk $H\downarrow$ was proposed in 1976 by Stwalley and Nosanow² as the best reliable option to achieve a Bose-Einstein condensate (BEC) state without the strong depletion of the condensate that correlations induce in superfluid ^4He . After 22 years of intense and continued experimental work by many groups, Fried *et al.*³ managed to achieve a BEC of $H\downarrow$. Problems that needed to be overcome included recombination on the walls, by working with a wall-free confinement, and low evaporation rates by using spin resonance. In the meantime, other BEC states were first achieved in 1995 working with alkali gases such as Rb, Na and Li.⁴

In contrast to alkali gases, the hydrogen-hydrogen interatomic interaction is very well known and leads to a stable gas phase. Spin-polarized hydrogen atoms interact via the triplet potential $b^3 \Sigma_u^+$ determined in an essentially exact way by Kolos and Wolniewicz,⁵ and recently extended to larger interparticle distances by Jamieson *et al.*⁶ The s-wave scattering length a is appreciably smaller than the typical values for alkalis, which retards evaporative cooling and produces a higher transition temperature ($50 \mu\text{K}$).

Essentially the same interaction can be applied for heavier isotopes spin-polarized deuterium $D\downarrow$ and tritium $T\downarrow$. $D\downarrow$ atoms obey Fermi statistics, and so the zero-pressure state of bulk $D\downarrow$ depends on the number of occupied nuclear spin states. In the limit of zero pressure and zero temperature, previous theoretical studies^{7,8,9} have shown that ($D\downarrow_1$) with only one occupied nuclear spin

state is a gas, while bulk $D\downarrow$ with two ($D\downarrow_2$) and three ($D\downarrow_3$) equally occupied nuclear spin states remains liquid. Spin-polarized tritium, which obeys Bose statistics, is expected to be liquid^{10,11,12} due to its larger mass. In fact, Stwaley and Nosanow² suggested it should behave very much like liquid ^4He and therefore constitute a second example of bosonic superfluid. Recently, microscopic properties of $T\downarrow$ clusters have been studied by Blume *et al.*¹³ using the diffusion Monte Carlo (DMC) method. In addition, in Ref. 13 spin-polarized tritium is suggested as a new BEC gas in optical dipole trap. It has the same advantage of a nearly exact knowledge of the interatomic potential as spin-polarized hydrogen but, unlike $H\downarrow$, it has a very broad Feshbach resonance that can be used to control the condensate in a trap.

In the present work, we present a DMC study of the liquid and solid phases of spin-polarized tritium. For bosonic many-body systems at zero temperature DMC methods lead to exact estimations of the ground-state energy and related properties within statistical errors. Using the *ab initio* $T\downarrow$ - $T\downarrow$ interatomic potential within the DMC method, we report accurate microscopic results for energetic and structural properties of the bulk system. Relevant results of this work include the determination of the equilibrium density and energy per particle, the spinodal point and the liquid-solid phase transition.

In Sec. II, we briefly describe the DMC method and the trial wave functions used for importance sampling in the liquid and solid phases. In Sec. III, the results of the DMC simulations are reported in several subsections. The first and second one are devoted to the microscopic results for the liquid and solid phases, respectively. In the last one, we study the liquid-solid phase transition point and report results on the freezing and melting densities. Finally, Sec. IV comprises a summary of our results and the main conclusions.

II. METHOD

The starting point of the DMC method is the Schrödinger equation written in imaginary time,

$$-\hbar \frac{\partial \Psi(\mathbf{R}, t)}{\partial t} = (H - E_r) \Psi(\mathbf{R}, t), \quad (1)$$

with an N -particle Hamiltonian

$$H = -\frac{\hbar^2}{2m} \sum_{i=1}^N \nabla_i^2 + \sum_{i<j}^N V(r_{ij}). \quad (2)$$

In Eq. (1), E_r is a constant acting as a reference energy and $\mathbf{R} \equiv (\mathbf{r}_1, \dots, \mathbf{r}_N)$ is a *walker* in Monte Carlo terminology. In order to reduce the variance to a manageable level it is a common practice to use importance sampling by introducing a trial wave function $\psi(\mathbf{R})$. Then, the Schrödinger equation is rewritten for the wave function $\Phi(\mathbf{R}, t) = \Psi(\mathbf{R}, t)\psi(\mathbf{R})$ and solved in a stochastic form. In the limit $t \rightarrow \infty$ only the lowest energy eigenfunction, not orthogonal to $\psi(\mathbf{R})$, survives and then the sampling of the ground state is effectively achieved. Apart from statistical uncertainties, the energy of a N -body bosonic system is exactly calculated.

The interaction between T \downarrow atoms is described with the spin-independent central triplet pair potential $b^3 \Sigma_u^+$. It has been determined in an essentially exact way by Kolos and Wolniewicz,⁵ and recently extended to larger interparticle distances by Jamieson *et al.* (JDW).⁶ As in a recent DMC calculation of bulk H \downarrow ,¹ we have used a cubic spline to interpolate between JDW data. This interaction is then smoothly connected to the long-range behavior of the T \downarrow -T \downarrow potential as calculated by Yan *et al.*¹⁴ The JDW potential used in the present work has a core diameter $\sigma = 3.67 \text{ \AA}$ and a minimum of -6.49 K at a distance 4.14 \AA . A comparison between different potentials employed in the past is reported in Ref. 1. We have also verified that the addition of mass-dependent adiabatic corrections (as calculated by Kolos and Rychlewski¹⁵) to the JDW potential does not change the energy of the bulk spin-polarized tritium.

The trial wave function used for the simulation of the liquid phase is of Jastrow form,

$$\psi_J(\mathbf{R}) = \prod_{i<j}^N f(r_{ij}). \quad (3)$$

The two-body correlation function $f(r)$ is the same as in our previous study of spin-polarized hydrogen,¹

$$f(r) = \exp[-b_1 \exp(-b_2 r)], \quad (4)$$

where b_1 and b_2 are variational parameters. The same form was also used in the variational Monte Carlo (VMC) calculation of Eters *et al.*,¹¹ who modeled the H \downarrow -H \downarrow interaction with a Morse potential fitted to reproduce Kolos and Wolniewicz *ab initio* data.⁵ This analytic form

(4) corresponds to the WKB solution of the two-body Schrödinger equation for small interparticle distances when the potential is of Morse type.

Simulations of the crystalline bcc, fcc and hcp phases have been also carried out; in this case, we use a Nosanow-Jastrow model

$$\psi_{\text{NJ}}(\mathbf{R}) = \psi_J(\mathbf{R}) \prod_i^N h(r_{iI}), \quad (5)$$

where $h(r) = \exp(-\alpha r^2/2)$ is a localizing function which links every particle i to a fixed lattice point \mathbf{r}_I . The parameter α is optimized variationally.

The trial wave function $\psi(\mathbf{R})$ has been optimized for the density range where the equation of state has been calculated, by using the VMC method. The liquid phase has been studied for densities in the interval from 0.006 \AA^{-3} to 0.02 \AA^{-3} . Within this interval, the value of the parameter b_1 (4) that optimizes the trial wave function takes increasing values with the density from 110 to 180, while the second parameter b_2 (4) does not change significantly, assuming values from 1.28 to 1.35 \AA^{-1} . For the three solid lattices (bcc, fcc and hcp), the calculations have been carried out from 0.008 to 0.024 \AA^{-3} . As in the case of the liquid phase, the parameter b_2 slightly changes, from 1.29 to 1.45 \AA^{-1} . The parameter b_1 increases with density from the melting point up to the highest density studied here, taking values from 80 to 148. The parameter α , which models the strength of the localization of particles around the lattice sites, increases with density. In the case of the bcc phase, optimized values of α range from 0.33 to 1.80 \AA^{-2} , for the fcc phase from 0.32 to 2.47 \AA^{-2} , and for the hcp phase from 0.28 to 2.21 \AA^{-2} . The statistical errors of the variational energies in this optimization procedure with VMC are compatible with those of the DMC results (see Tables I and II).

We use the DMC method accurate to second order in the time step Δt ,¹⁶ which allows us to use larger Δt values than in linear DMC. Both the time-step dependence and the mean walker population have been studied carefully in order to eliminate any bias coming from them.

Any simulation of a bulk system with a finite number of particles requires a size-dependence analysis in order to achieve results as close as possible to the thermodynamic limit. For the liquid phase, we have used 250 particles in all simulations and checked at the VMC level that with the addition of standard tail corrections, the size dependence of the energy remains smaller than the typical size of the statistical error. On the other hand, in all the solid state simulations we have assumed periodic boundary conditions, with 256, 250, and 180 atoms for the bcc, fcc, and hcp lattices, respectively. Due to the periodic order of the solid, standard tail corrections which assume $(g(r) = 1)$ beyond $r > L/2$, where L is the length of the simulation box, become rather inaccurate. In order to better determine the energy tail corrections we have studied the size dependence of the energy at the

ρ (\AA^{-3})	E/N (K)	T/N (K)	P (bar)	c (m/s)
0.006	-3.427(2)	5.578(17)	-1.43(2)	71(3)
0.0074	-3.664(6)	7.778(18)	-0.12(1)	189(3)
0.009	-3.320(7)	10.84(3)	5.11(6)	318(3)
0.01	-2.675(8)	13.06(4)	11.6(1)	402(4)
0.0125	0.86(2)	19.28(6)	45.2(4)	630(5)
0.016	12.26(6)	30.33(10)	161(2)	992(8)

TABLE I: Results for liquid T \downarrow at different densities ρ : energy per particle (E/N), kinetic energy per particle (T/N), pressure (P), and speed of sound (c). Figures in parenthesis are the statistical errors.

VMC level, where larger number of particles can be used. From the VMC results one extracts the tail corrections for a given number of atoms and then these are added to the DMC energies. With this procedure it was possible to reproduce accurately the experimental equation of state of solid ${}^4\text{He}$ ¹⁷.

III. RESULTS

A. Liquid phase

Spin-polarized T in its liquid phase has been studied in the density range from spinodal point up to densities above crystallization. DMC results for the total and kinetic energy per particle at different densities are reported in Table I. In order to remove any residual bias from the trial wave function, kinetic energies are calculated as differences between total energies and pure estimations of potential energies. The total energy is negative approximately up to the density $\rho = 0.012 \text{ \AA}^{-3}$. The potential energy per particle is negative in all the density regime studied, presenting a minimum value of around -19 K at the density $\rho = 0.014 \text{ \AA}^{-3}$.

In Fig. 1, we plot the DMC results for the equation of state of the liquid. We have tried different analytical forms to fit the DMC data. The best results have been obtained by using a polynomial fit of the form ($e \equiv E/N$)

$$e(\rho) = e_0 + B \left(\frac{\rho - \rho_0}{\rho_0} \right)^2 + C \left(\frac{\rho - \rho_0}{\rho_0} \right)^3, \quad (6)$$

ρ_0 and e_0 being the equilibrium density and the energy per particle at this density, respectively. The equation of state (6) is shown as a solid line on top of the DMC data in Fig. 1. The best set of parameters is: $e_0 = -3.656(4)$ K, $B = 6.86(7)$ K, $C = 4.70(5)$ K, and $\rho_0 = 0.007466(7) \text{ \AA}^{-3}$, the figures in parenthesis being the statistical uncertainties. It is worth noticing that the value obtained for the equilibrium density expressed in units of σ^{-3} , $\rho_0 = 0.369 \sigma^{-3}$ ($\sigma = 3.67 \text{ \AA}$) is similar to the one in liquid ${}^4\text{He}$, $\rho_0 = 0.365 \sigma^{-3}$ ($\sigma = 2.556 \text{ \AA}$).

Using the equation of state (6), we have obtained the

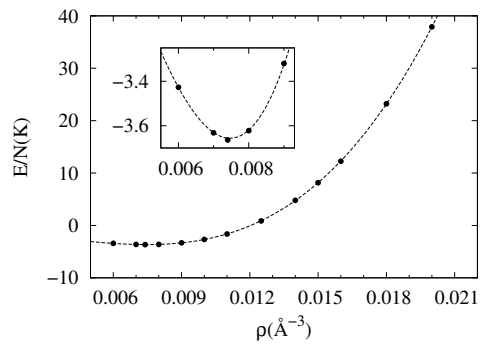


FIG. 1: Energy per particle of liquid T \downarrow (solid circles) as a function of the density ρ . The solid line corresponds to the fit to the DMC energies using Eq. (6). The error bars of the DMC energies are smaller than the size of the symbols.

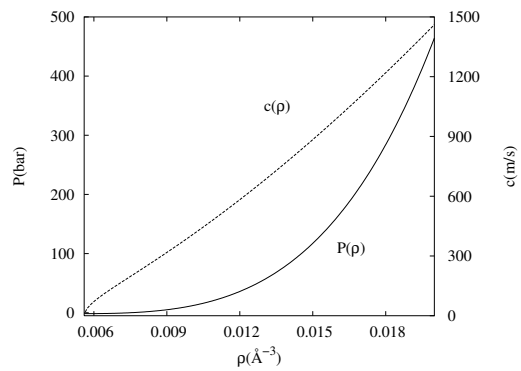


FIG. 2: Pressure and speed of sound of liquid T \downarrow as a function of the density. Left (right) scale corresponds to pressure (speed of sound).

pressure from its thermodynamic definition

$$P(\rho) = \rho^2 (\partial e / \partial \rho); \quad (7)$$

and from it, the corresponding speed of sound as a function of the density

$$c^2(\rho) = \frac{1}{m} \left(\frac{\partial P}{\partial \rho} \right). \quad (8)$$

In Table I, we report results for the pressure P and the speed of sound c for some values of the density, where specific DMC simulations have been carried out. The functions $P(\rho)$ and $c(\rho)$, derived respectively from Eqs. (7) and (8), are shown in Fig. 2.

The spinodal density in T \downarrow , i.e., the density where the speed of sound becomes zero, is $\rho_0 = 0.0056 \text{ \AA}^{-3} = 0.277 \sigma^{-3}$, corresponding to a pressure of $P_s = -1.48(2)$ bar. For comparison, the spinodal density in liquid ${}^4\text{He}$ is a bit lower, $\rho_0 = 0.264 \sigma^{-3}$, the spinodal pressure being larger in absolute value, $P_s = -9.30(15)$ bar. In Fig. 3, we plot the speed of sound c (8) as a function of the pressure for pressures approximately up to solidification. It can be seen that c drops very fast when approaching

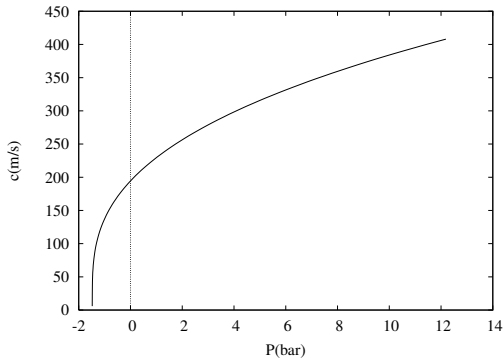


FIG. 3: Speed of sound of liquid $T\downarrow$ as a function of the pressure from the spinodal point up to freezing. The spinodal pressure P_s corresponds to the point where $c = 0$.

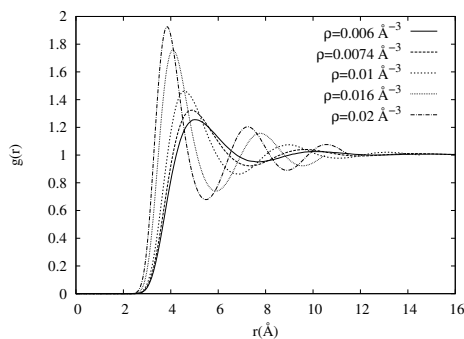


FIG. 4: Two-body radial distribution functions of the liquid phase. From bottom to top in the height of the main peak, the results correspond to densities 0.006, 0.0074, 0.01, 0.016, and 0.02 \AA^{-3} .

the spinodal point. Near the spinodal point it is expected that c has the form $\propto (P - P_s)^{1/\nu}$, where ν is the critical exponent.

Apart from the ground-state energy, DMC simulations enables us to make exact estimations of other relevant magnitudes such as the two-body radial distribution function $g(r)$ and its Fourier transform, the static structure function $S(k)$. The use of pure estimators¹⁸ eliminates the bias coming from the trial wave function and allows us to arrive to exact results for both functions. The evolution of $g(r)$ with density for liquid $T\downarrow$ is shown in Fig. 4. It is very similar to the well-known results for liquid ${}^4\text{He}$. When ρ increases, $g(r)$ gains structure, with the main peak shifting to shorter distances and increasing its strength.

In Fig. 5, results of $S(k)$ at the same densities as in Fig. 4 are reported. The results again show the expected behavior: with the increase of ρ , the strength of the main peak increases and moves to higher momenta in a monotonic way. At low momenta, the slope of $S(k)$ decreases with the density, following the limiting behavior $\lim_{k \rightarrow 0} S(k) = \hbar k / (2mc)$ driven by the speed of sound c . The DMC data start at a finite k value inversely propor-

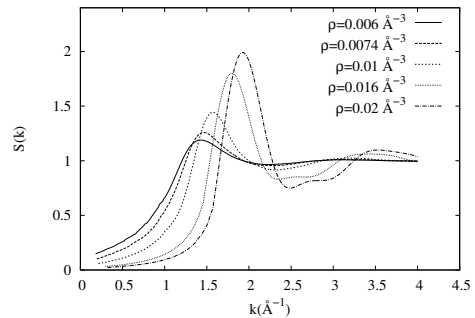


FIG. 5: Static structure function of the liquid phase. From bottom to top in the height of the main peak, the results correspond to densities 0.006, 0.0074, 0.01, 0.016, and 0.02 \AA^{-3} .

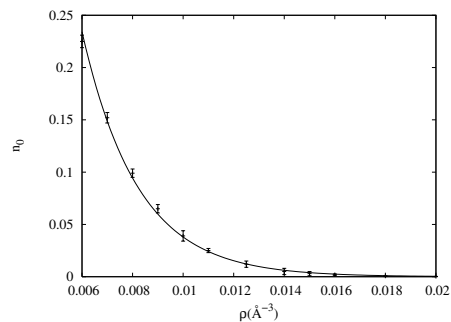


FIG. 6: Condensate fraction of spin-polarized T in the liquid phase. The line corresponds to a fit to the DMC data using Eq.(9). The error bars are smaller than the size of the symbols.

tional to the box size L .

A characteristic signature of bulk superfluidity is the finite value of the condensate fraction n_0 , i.e. the fraction of particles occupying the zero-momentum state. It has been extracted from the long-range behavior of the one-body density matrix $\rho(r)$, by means of the asymptotic condition $n_0 = \lim_{r \rightarrow \infty} \rho(r)$. We have verified, by increasing the number of particles of the simulation at different densities, that the size dependence of n_0 is smaller than its statistical error. The results obtained using the extrapolated estimator $n_0 \simeq 2\langle n_0 \rangle_{\text{DMC}} - \langle n_0 \rangle_{\text{VMC}}$ are presented in Fig. 6. The line on top of the data corresponds to the exponential fit

$$n_0(\rho) = A \exp(-b\rho) \quad (9)$$

with $A=3.6(3)$ and $b=455(11) \text{\AA}^{-1}$, which describes well the DMC data. At the equilibrium density, $n_0=0.129(3)$. For comparison, ${}^4\text{He}$ at the equilibrium has $n_0=0.084(1)$, as obtained by the DMC method using a Jastrow wavefunctions for importance sampling in Ref. 16.

Previous theoretical estimates of the energy per particle in bulk tritium were obtained by VMC¹¹ or Brueckner-Bethe-Goldstone formalism.¹² The $T\downarrow$ - $T\downarrow$ interaction was modeled with the Morse potential and the

calculations were performed for densities up to 0.015 \AA^{-3} . Eters *et al.*¹¹ obtained an equilibrium energy per particle $E/N = -0.75(2)$ K for the equilibrium density $\rho_0 = 0.0463 \text{ \AA}^{-3}$. For the same density, Joudeh *et al.*¹² obtained -0.759 K. Comparing this equilibrium density with the present DMC results one notices that this variational estimate lies below our estimated spinodal point. In order to compare our results with previous ones, we have carried out simulations at a density $\rho = 0.005 \text{ \AA}^{-3}$ using both the Morse potential and the JDW one. With the Morse potential and at the VMC level we obtain $E/N = -0.74(1)$ K, which is within the errorbars the same result as that of Eters *et al.* ($-0.75(2)$ K). Using the Morse potential, the DMC calculation lowers the energy to $-0.978(1)$ K. At the same density 0.005 \AA^{-3} , we have also used the JDW potential obtaining at the DMC level a sizeable lower energy of $-2.900(2)$ K. The observed differences in the equation of state imply also substantial changes in the estimated pressure and compressibility. For example, for a density $\rho = 0.01 \text{ \AA}^{-3}$ we find a pressure of $11.6(1)$ bar, while in Ref. 11 it is estimated to be 17 bar. At higher densities, the difference between the pressure results grows, amounting to approximately 80 bar at 0.015 \AA^{-3} .

Using the relation for the transition temperature of the ideal Bose-Einstein gas

$$T_c = 3.31 \left(\frac{\hbar^2}{mk_B} \right) \rho_0^{2/3}, \quad (10)$$

Eters *et al.*¹¹ estimated the temperature of superfluid transition of spin-polarized T to be 1.48 K. With the same argument, our results for the equilibrium density suggest a superfluid transition temperature of 2.02 K. This is of course only an approximate estimation since in liquid ^4He Eq. 10 gives 3.1 K instead of the right one of 2.17 K.

B. Solid phase

We have performed calculations of the spin-polarized T solid phase with three different lattices (bcc, fcc, hcp) and using the Nosanow-Jastrow wave function (5) for importance sampling. The energy per particle in bcc, fcc, and hcp lattices has been obtained for different densities in the range from 0.008 \AA^{-3} to 0.024 \AA^{-3} . Our DMC results show that the energies per particle for the three lattices are statistically indistinguishable in all the studied density regime. Still, it reaches the lowest values in the hcp solid phase, so this lattice seems to be energetically preferred. As an example, the results at two densities for bcc, fcc and hcp lattices are respectively: for $\rho = 0.011 \text{ \AA}^{-3}$, near the melting density, the energies per particle are $E/N = -1.96(5)$, $-1.98(7)$, and $-2.04(6)$ K; at a higher density $\rho = 0.018 \text{ \AA}^{-3}$, $E/N = 15.8(2)$, $15.3(2)$, and $15.26(8)$ K. The same behavior has been observed for all densities and therefore we decided to investigate solid

ρ (\AA^{-3})	E/N (K)	T/N (K)	P (bar)	c (m/s)
0.01	-2.56(6)	14.16(8)	4.7(7)	321(18)
0.011	-2.04(6)	16.51(9)	11(1)	404(19)
0.015	4.17(8)	27.89(11)	83(4)	782(28)
0.018	15.26(8)	38.30(12)	218(8)	1113(36)
0.024	62.59(8)	62.54(13)	902(29)	1898(58)

TABLE II: Results for solid T \downarrow at different densities ρ : energy per particle (E/N), kinetic energy per particle (T/N), pressure (P), and speed of sound (c). Figures in parenthesis are the statistical errors.

T \downarrow properties assuming its hcp crystalline structure. It is important to notice that the bcc lattice proved to be energetically preferred in a recent study of the gas-solid phase transition in H \downarrow ¹ as well as in a study of solid hydrogen at very high pressure¹⁹.

In Fig. 7, the DMC energies per particle of the solid phase at different densities have been shown, for the three lattices. The line on top of the data in the figure corresponds to the equation of state of the solid hcp lattice. It has been obtained by fitting the DMC results with a polynomial function of the form

$$e(\rho) = s_2\rho^2 + s_3\rho^3 + s_4\rho^4, \quad (11)$$

with parameters $s_2 = -10.47(11) \times 10^4 \text{ K}\text{\AA}^2$, $s_3 = 7.13(15) \times 10^6 \text{ K}\text{\AA}^3$, and $s_4 = 7.3(5) \times 10^7 \text{ K}\text{\AA}^4$.

The total and kinetic energies per particle for several selected densities are given in Table II. Kinetic energy is determined in the same way as in the liquid phase. The total energy is negative for $\rho \leq 0.012 \text{ \AA}^{-3}$, while for greater densities the kinetic energy exceeds the absolute value of the potential one causing the total energy to become positive. The potential energy is negative for all the considered densities, with a single exception corresponding to the highest density 0.024 \AA^{-3} . As it is reported in Ref. 1, the smaller mass of H \downarrow atoms caused the potential energy to enter in regime of positive values for slightly smaller densities ($\rho \geq 0.02 \text{ \AA}^{-3}$).

In Fig.8, we show the pressure and speed of sound of solid T \downarrow obtained from the equation of state (11) using the thermodynamic relations (7) and (8) as a function of the density. Comparison with values of the same quantities in solid bulk H \downarrow , reported in Ref. 1, reveals smaller pressure and speed of sound for solid T \downarrow at the same densities.

The spatial pattern of the solid structure is reflected in the two-body radial distribution function $g(r)$. In Fig. 9, we have plotted $g(r)$ for some selected densities. The strength of the main peaks are greater in the solid than in the liquid phase, as can be seen by comparison of our results at densities 0.01 \AA^{-3} and 0.02 \AA^{-3} . Also, it is clear that secondary peaks are larger in the solid phase. Just like in the liquid, when the density increases the height of the main peaks grows and moves to shorter distances.

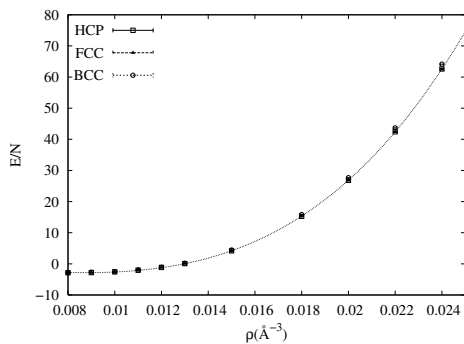


FIG. 7: Energy per particle of solid $T\downarrow$ as a function of the density ρ for the hcp (boxes), fcc(triangles) and bcc(circles) lattices. The solid line corresponds to the fit to the DMC energies using Eq. (11). The error bars of the DMC energies are smaller than the size of the symbols.

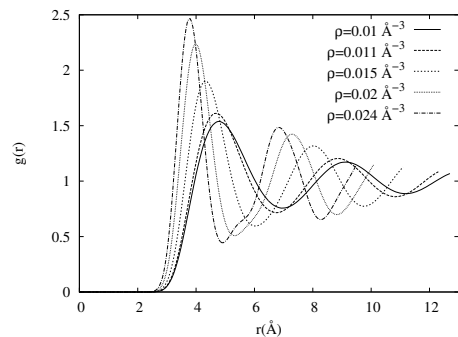


FIG. 9: Two-body radial distribution functions of the solid phase. From bottom to top in the height of the main peak, the results correspond to densities 0.01, 0.011, 0.015, 0.02 and 0.024 \AA^{-3} .

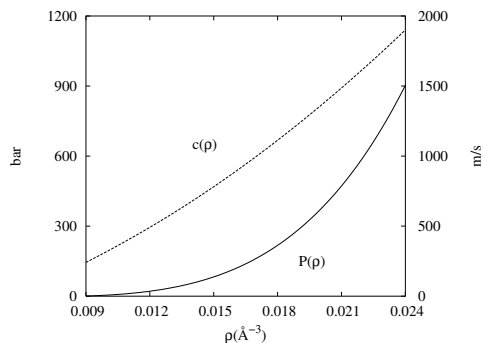


FIG. 8: Pressure and speed of sound of solid $T\downarrow$ as a function of the density. Left (right) scale corresponds to pressure (speed of sound).

C. Liquid-solid phase transition

An important information that can be derived from the DMC simulations of the liquid and solid phases is the location of the liquid-solid phase transition point. As in a recent investigation of the gas-solid phase transition in $H\downarrow^1$, we have used the double-tangent Maxwell construction to determine the transition. This well-known method is based on the search of a common tangent to both the liquid and solid equations of state whose intersections give the freezing (ρ_f) and melting (ρ_m) densities, as plotted in Fig. 10. Using the equation of state of the hcp crystalline structure, we have obtained $\rho_f = 0.00964 \text{\AA}^{-3} = 0.477 \sigma^{-3}$ and $\rho_m = 0.01069 \text{\AA}^{-3} = 0.528 \sigma^{-3}$, which corresponds to a common pressure at the phase transition of $P = 9(1)$ bar. In addition, in order to estimate the influence of the lattice type on the transition pressure, we have also calculated the transition densities and pressure for fcc and bcc lattices. For a fcc lattice $P = 9.5(1.0)$ bar, while for bcc we have obtained $P = 9.9(1.0)$ bar. The three transition pressures fall within the errorbars, but since hcp is consistently lower than the others it leads us to conclude that

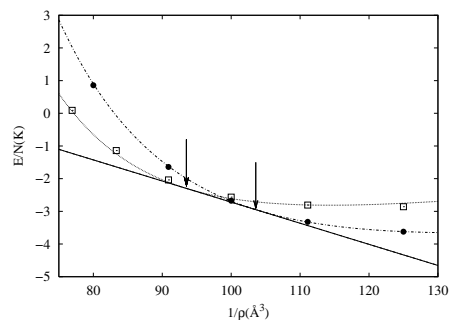


FIG. 10: Maxwell construction based on plotting the energy per particle, E/N as a function of $1/\rho$. The densities at which the first-order transition occurs are identified by finding the common tangent (solid line) to both the solid (dotted line) and liquid curve (dot-dashed line).

it may be slightly preferred, like it is preferred in ^4He . The transition densities in ^4He are $\rho_f = 0.430 \sigma^{-3}$ and $\rho_m = 0.468 \sigma^{-3}$,²⁰ corresponding to a pressure of 25.3 bar. The comparison can also be made with with gas-solid transition in spin-polarized $H\downarrow^1$. In this case, the phase transition occurs at higher densities $\rho_f = 0.01328 \text{\AA}^{-3}$, $\rho_m = 0.01379 \text{\AA}^{-3}$ and much higher pressure, $P = 173(15)$ bar, than in spin-polarized T. This effect can be explained as a consequence of its isotopic difference since $T\downarrow$ atoms have approximately three times greater mass than $H\downarrow$ atoms.

As in any first-order phase transition, the density is discontinuous in the transition point. Another quantity which is also not continuous crossing the phase transition is the kinetic energy per particle. Namely, near the freezing density the kinetic energy per particle of the liquid is $T/N = 13.06(3)$ K, while at the same time, near the melting density but in the solid phase the same energy is $T/N = 16.51(3)$ K. Therefore, our results for bulk $T\downarrow$ show a discontinuity of the kinetic energy of around 3.5 K; in bulk $H\downarrow$, the same difference has been shown to be more than twice times larger.¹ On the other hand, the value of the condensate fraction in the two spin-polarized

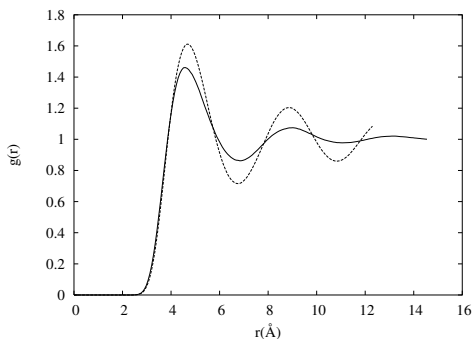


FIG. 11: Two-body radial distribution function at the liquid-solid phase transition. The solid line corresponds to the liquid at ρ_f and the dashed line to the solid at ρ_m .

systems at the corresponding transition densities are similar, 0.03 for $T\downarrow$ and 0.04 for $H\downarrow$ ¹.

A measure of the mean displacement of $T\downarrow$ atoms with respect to the lattice sites is obtained by computing the Lindemann's ratio (γ). As usual, we calculate it by sampling the expression $\gamma = \sqrt{\langle(\mathbf{r} - \mathbf{r}_I)^2\rangle}/a_L$, where a_L is the lattice constant. The parameter γ decreases monotonically with increasing density and the values we have obtained show a slight dependence on the particular lattice chosen for the simulation: it is greatest for hcp and smallest for bcc. Particularly, at the melting density of the hcp phase Lindemann's ratio assumes a value $\gamma = 0.26$, which is the same as in ${}^4\text{He}$ and similar to the value estimated for solid $H\downarrow$ ($\gamma = 0.25$)¹.

The discontinuity in the liquid-solid transition is also revealed in the difference between $g(r)$ of the liquid and solid phases (Fig. 11). Even more dramatic difference between the two phases is demonstrated in Fig. 12 where DMC results of $S(k)$ are shown at ρ_f and ρ_m . $S(k)$ in the solid phase is characterized with strong peaks at reciprocal lattice sites whereas this behavior is clearly not observed in the $S(k)$ of the liquid phase. Finally, it is worth noticing that the main peak of solid $S(k)$ is slightly weaker in $T\downarrow$ than in $H\downarrow$ (reported in Ref. 1). The main reason for this lies in the fact that the liquid-solid transition in $T\downarrow$ emerges at lower densities than gas-solid transition in $H\downarrow$.

IV. CONCLUSIONS

The ground-state properties of spin-polarized tritium $T\downarrow$ have been accurately determined using the DMC method in both the liquid and solid phases. The obtained results are based on the precise knowledge of the $T\downarrow$ - $T\downarrow$ interatomic potential, which combined with the accuracy of the DMC method, allowed for a nearly ex-

act determination of the main properties of the system. All the previous results on liquid $T\downarrow$ were based on a Morse potential and approximate computational methods. Hence, our predictions for equilibrium density and

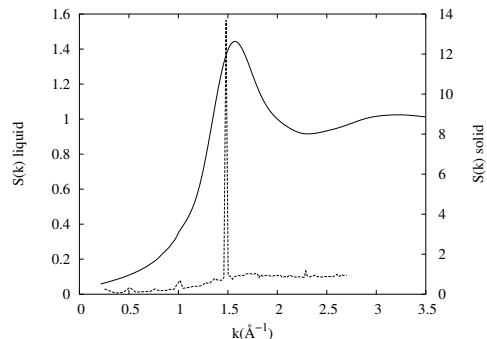


FIG. 12: Static structure factor at the liquid-solid phase transition. The results correspond to the liquid at ρ_f and to the solid at ρ_m .

energy per particle differ substantially from those. We find that the equilibrium density is $\rho_0 = 0.00747(1) \text{ \AA}^{-3}$, which expressed in units of σ^{-3} is very similar to the one of liquid ${}^4\text{He}$ ($\rho_0 = 0.369 \sigma^{-3}$ for $T\downarrow$, $\rho_0 = 0.365 \sigma^{-3}$ in ${}^4\text{He}$). Previous predictions of the equilibrium density lie below our predicted spinodal density. Despite a similar equilibrium density, $T\downarrow$ has approximately half the equilibrium energy per particle of liquid ${}^4\text{He}$ as a consequence of its smaller mass and shallower potential.

At a high enough density the system freezes. We have studied the energetic and structural properties of the solid phase for three lattices. Differences in energies between the phases are almost indistinguishable, but hcp seems to be slightly preferred over the fcc and bcc ones. From the DMC equations of state of the liquid and solid phases, we have localized the liquid-solid transition point of $T\downarrow$ for the first time, to the best of our knowledge. At zero temperature, the phase transition occurs at $P = 9(1)$ bar.

Acknowledgments

J. B. acknowledges support from DGI (Spain) Grant No. FIS2008-04403 and Generalitat de Catalunya Grant No. 2005SGR-00779. I.B. and L.V.M. acknowledge support from MSES (Croatia) under Grant No. 177-1770508-0493. We also acknowledge the support of the Central Computing Services at the Johannes Kepler University in Linz, where part of the computations was performed. In addition, the resources of the Isabella cluster at Zagreb University Computing Centre (Srce) and Croatian National Grid Infrastructure (CRO NGI) were used.

¹ L. Vranješ Markić, J. Boronat and J. Casulleras, Phys. Rev. B **75**, 064506 (2007).

² W. C. Stwaley and L. H. Nosanow, Phys. Rev. Lett. **36**,

- 910 (1976).
- ³ D. G. Fried *et. al.*, Phys. Rev. Lett. **81**, 3811 (1998).
- ⁴ M. H. Anderson, J. R. Ensher, M. R. Matthews, C. E. Wieman, and E. A. Cornell, Science **269**, 198 (1995); K. B. Davis, M. O. Mewes, M. R. Andrews, N. J. van Druten, D. S. Durfee, D. M. Kurn, and W. Ketterle, Phys. Rev. Lett. **75**, 3969 (1995); C. C. Bradley, C. A. Sackett, J. J. Tollett, and R. G. Hulet, Phys. Rev. Lett. **75**, 1687 (1995).
- ⁵ W. Kolos and L. Wolniewicz, J. Chem. Phys. **43**, 2429 (1965); Chem. Phys. Lett. **24**, 457 (1974).
- ⁶ M. J. Jamieson, A. Dalgarno, and L. Wolniewicz, Phys. Rev. A **61**, 042705 (2000).
- ⁷ R. M. Panoff and J. W. Clark, Phys. Rev. B **36** 5527 (1987)
- ⁸ M. F. Flynn, J. W. Clark, E. Krotscheck, R. A. Smith, and R. M. Panoff, Phys. Rev. B **32**, 2945 (1985).
- ⁹ B. Skjetne and E. Østgaard, J. Phys.: Condens. Matter **11** 8017 (1999).
- ¹⁰ M. D. Miller, L. H. Nosanow, Phys. Rev. B **15**, 4376 (1977).
- ¹¹ R. D. Etters, J. V. Dugan, Jr., and R. W. Palmer, J. Chem. Phys. **62**, 313 (1975).
- ¹² B. R. Joudeh, M. K. Al-Sugheir, H. B. Ghassib, Physica B **388**, 237 (2007).
- ¹³ D. Blume, B. D. Esry, Chris H. Greene, N. N. Klausen, and G. J. Hanna, Phys. Rev. Lett. **89**, 163402 (2002).
- ¹⁴ Zong-Chao Yan, James F. Babb, A. Dalgarno, and G. W. F. Drake, Phys. Rev A **54**, 2824(1996).
- ¹⁵ W. Kolos and J. Rychlewski, J. Mol. Spectrosc. **143**, 237 (1990).
- ¹⁶ J. Boronat and J. Casulleras, Phys. Rev. B **49** 8920 (1994).
- ¹⁷ L. Vranješ, J. Boronat, J. Casulleras, and C. Cazorla, Phys. Rev. Lett. **95** 145302 (2005).
- ¹⁸ J. Casulleras and J. Boronat, Phys. Rev. B **52**, 3654 (1995).
- ¹⁹ C. Pierleoni, D. M. Ceperley, and M. Holzmann, Phys. Rev. Lett. **93**, 146402 (2004).
- ²⁰ D. O. Edwards and R. C. Pandorff, Phys. Rev. A **140**, 816 (1965).